*Progress In Electromagnetics Research M, Vol. 40, 153–166, 2014*

# Digital Beamforming on Receive in Elevation for Spaceborne Hybrid Phased-MIMO SAR

**Lele Zhang and Dianren Chen***

**Abstract**—This paper proposes an imaging method of multi-direction swath and digital beamforming (DBF) in elevation for spaceborne Hybrid Phased-MIMO SAR that combines traditional phased-array radar with a new technique for multiple-input multiple-output (MIMO) radar to achieve multifunctional synthetic aperture radar (SAR). At first, we build a signal model and derive a virtual control matrix of the Hybrid Phased-MIMO SAR. Furthermore, considering the image overlap and range ambiguity caused by multiple direction imaging, we present adaptive Digital Beamforming based on Linearly Constrained Minimum Variance (LCMV). In this approach, the first constraint is dedicated to make the overall beamformer response equal the quiescent response in the desired signal region so that the signal is not cancelled when it is present, and additional constraints are included to assure proper reception of the desired signal and form nulls in the direction of interference at the same time. The diagonal loading method is combined with this method to reduce small eigenvalue interference for its eigenvector, which improves the convergence speed in sidelobe. The substantial improvements offered by the proposed adaptive Digital Beamforming technique as compared to previous techniques are demonstrated analytically and by simulations through analysis of the corresponding range compression results and achievable output performance of interference suppression. Simulation results validate the effectiveness of the adaptive DBF.

## 1. INTRODUCTION

Compared with traditional spaceborne synthetic aperture radar (SAR), the next generation of top-level spaceborne SAR systems will comprise, among others, high resolution and long-range imaging capabilities, highly sensitive ground moving target indication and a multitude of sophisticated operational modes including multi-beam ScanSAR, Terrain Observation by Progressive Scans (TOPS), Spotlight and high-resolution wide-swath (HRWS) [1–5]. In some applications, more satellites are required for dynamic monitoring of the same ground area and precision tracking or velocity measurements of special moving target [6]. However, to achieve these forthcoming radar tasks with one SAR satellite demands multi-direction swath imaging. In [7], a totally novel concept, bidirectional SAR (BiDi SAR) imaging mode, was put forward as a practical means in the TerraSAR-X system. The BiDi imaging is to achieve the simultaneous imaging of two directions based on an azimuth pattern with two major lobes pointing into different directions. Because of little flexibility and antenna limitation with the use of main lobe and one grating lobe, it cannot work well in the range and azimuth direction at the same time.

The promising concept of reflector antennas in conjunction with digital feed arrays is exploited for future SAR systems. The innovative system allows flexible data handling and implementation of DBF concepts [8–10]. Phased Array Multifunctional Imaging Radar (PAMIR) was proposed in [11] as a potential method to meet the growing demands for future reconnaissance systems with respect to

*Received 13 November 2014, Accepted 18 December 2014, Scheduled 7 January 2015*
* Corresponding author: Dianren Chen (dianrenchen@cust.edu.cn).
The authors are with the School of Electronics and Information Engineering, Changchun University of Science and Technology, Changchun 130022, China.

flexibility and multimode operation. The paper by Ludwig et al. [12] discusses the status in Europe of active array antennas for space applications and trends for next generation instruments with a view to cost reduction and new applications. Although the real price of spaceborne phased array radar and radar data generated with the available instrument technology of today is too high, affordable operational instruments will play a key role in the very near future. Multiple-input multiple-output (MIMO) radar system with multidimensional waveform encoding [13–15] is to employ multiple antennas for emitting several orthogonal waveforms which is better than traditional phased-array radar, but loosing coherent processing gain at the transmitting array. Recently, a compromise formulation between the coherent processing gain offered by the phased-array radar and the advantages of the MIMO radar, e.g., the waveform diversity, was proposed and named as Hybrid MIMO Phased Array Radar (HMPAR) [16–20]. HMPAR is to partition the transmitting array into multi-arrays which is allowed to overlap, and each of these subarrays is in turn used to emit the orthogonal signal through transmitting beamforming towards arbitrary direction in space.

In order to satisfy the requirements of the multifunctional spaceborne synthetic aperture radar, this paper combines HMPAR with SAR and terms spaceborne Hybrid Phased-MIMO SAR. We propose an advanced multi-direction swath imaging approach based on spaceborne Hybrid Phased-MIMO SAR. Nevertheless, since subpulses that can be achieved by dividing a long pulse are transmitted successively, echoes of these subpulses will inevitably overlap in a certain receiving period. Multi-direction swath imaging undoubtedly causes a number of range ambiguities. But the scattered signals from different subpulses will then, at each instant of time, arrive from different elevation angles, and it becomes possible to separate the radar echoes from different subpulses by digital beamforming on receive in elevation. The motivation for using DBF techniques is its ability to provide a wide swath and high resolution simultaneously. A novel finite-impulse response (FIR) processing network was proposed to improve separation performance [21]. But the performance improvement is not obvious compared with conventional null-steering beamforming. In [22], three methods of radar echoes separation are introduced, and their theorem is similar to the well-known convolution theorem, which states that the cross-correlation of two functions can be expressed in the frequency domain via the product of their individual Fourier transforms. However, they must ensure that arbitrary shifts between the transmit signals are orthogonal, and these signals have non-overlapping spectral. This paper presents an advanced adaptive DBF algorithm based on Linearly Constrained Minimum Variance (LCMV) and derives optimal weights by adding additional constraints to guarantee proper reception of the desired signal and deep suppression of interference signal. Simulation results demonstrate that this algorithm can suppress interference signal effectively and stably, so as to separate overlapped echoes from each subpulse.

This paper is organized as follows. Section 2 reviews the principle for HMPAR. In Section 3, signal model of the Hybrid Phased-MIMO SAR (Section 3.1), advanced algorithm of adaptive DBF in elevation (Section 3.2), system design of the Hybrid Phased-MIMO SAR (Section 3.3) are presented. We turn the focus to build a signal model of the Hybrid Phased-MIMO SAR and find the optimal weight vector to ensure a reliable separation between echoes from different subpulses and set nulls at the range ambiguity direction. Simulation experiment is performed in Section 4, where we compare the performance of our method with that of conventional beamformings. Section 5 concludes this paper with a short summary.

## 2. PRINCIPLE FOR HMPAR

In the following, the innovative HMPAR will be illustrated which is the combination of MIMO and phase-array radar. There is a rectangular array that can be referred to as $MN$ array, organized into $M$ subarrays of $N$ elements each, as shown in Fig. 1. Other configurations are also possible. Every subarray will produce a beampattern that illuminates a fraction $1/M$ of the total search volume, and if the beams are forming appropriately, transmit energy will be distributed evenly for the entire search volume. When all $M$ signals are perfectly correlative and all $M$ subarrays pointed in the same direction, HMPAR acts as one large phased array. There are many different configurations with respect to the requirements of different applications, so that the transmit beampatterns will afford the greatest flexibility. We will often use the case $M = N$ because of its most flexibility in transmit beampattern design. For example, the subarrays can be $5 \times 4$, and the meta-array will form a $4 \times 5$ grid. The full set of possible rectangular

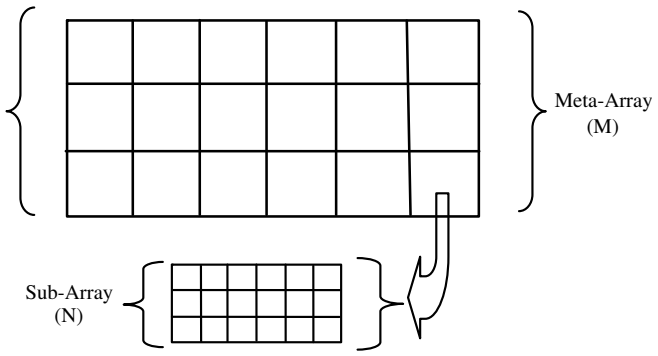


**Figure 1.** HMPAR notional concept.

configurations in $M = N$=20 case is in Table 1.

**Table 1.** Possible rectangular configuration.

| Meta-Array ($M$) | $20 \times 1$ | $10 \times 2$ | $5 \times 4$ | $1 \times 20$ | $2 \times 10$ | $4 \times 5$ |
|---|---|---|---|---|---|---|
| Sub-Array ($N$) | $1 \times 20$ | $2 \times 10$ | $4 \times 5$ | $20 \times 1$ | $10 \times 2$ | $5 \times 4$ |

HMPAR combines the merits of phased-array radar and MIMO radar. We will derive the theory model of transmit signal of the HMPAR through the analysis of the respective merits. Suppose that the waveform vector $\tilde{\mathbf{s}}(t) = [\ \tilde{s}_1(t) \quad \dots \quad \tilde{s}_M(t)\ ]$ includes $M$ orthogonal signals with each other, and signal covariance matrix can then be expressed as

$$\mathbf{R}(0) = \int_{T_d} \tilde{\mathbf{s}}(t)\, \tilde{\mathbf{s}}^H(t)\, dt = \mathbf{I}_M \tag{1}$$

where $\mathbf{I}_M$ is the $M \times M$ identity matrix, $T_d$ the radar pulse width, $(\cdot)^H$ the Hermitian transpose, and the total transmit power is given by

$$E = trace\left\{ \int_{T_d} \tilde{\mathbf{s}}(t)\, \tilde{\mathbf{s}}^H(t)\, dt \right\} = M \tag{2}$$

where $trace\{\cdot\}$ is the trace of a matrix, and the signal transmitted by the $k$th subarray can be modeled as

$$\mathbf{s}_k(t) = \sqrt{E_k}\tilde{s}_k(t)\, \mathbf{w}_k^*, \quad k = 1, \dots, M \tag{3}$$

where $(\cdot)^*$ denotes the conjugate operator, and $\mathbf{w}_k$ is the unit-norm complex vector of beamforming weights associated with the $k$th subarray defined as

$$\mathbf{w}_k = \frac{\mathbf{a}_k(\theta_k)}{\|\mathbf{a}_k(\theta_k)\|}, \quad k = 1, \dots, M \tag{4}$$

$E_k$ is the energy of the $k$th subpulse with its definition of

$$E_k = \int_{T_d} \mathbf{s}_k^H(t)\, \mathbf{s}_k(t)\, dt = \frac{M}{M} = 1 \tag{5}$$

If every beam formed by each of $M$ subarrays is pointed in different directions, the steering vector of every subarray and the steering vector matrix of HMPAR are

$$\mathbf{a}_k(\theta_k) = \left[\ 1 \quad e^{-j(2\pi f_0 d \cos\theta_k / c)} \quad \dots \quad e^{-j(2\pi f_0 (N-1) d \cos\theta_k / c)}\ \right]^T \tag{6}$$

$$\mathbf{A}(\theta) = [\ \mathbf{a}_1(\theta_1) \quad \dots \quad \mathbf{a}_M(\theta_M)\ ] \tag{7}$$

where $f_0$, $c$ and $d$ denote the carrier frequency, the speed of light, element spacing, respectively. $\theta_k$ is the beam direction formed by the $k$th subarray and $(\cdot)^T$ the transpose. The total transmit signal is

$$y(t) = \sum_{k=1}^{M} \sqrt{E_k}\tilde{s}_k(t)\, \mathbf{w}_k^H \mathbf{a}_k(\theta_k) \tag{8}$$

It is indicated that the system illuminates $M$ different directions at the same time by emitting $M$ orthogonal signals through $M$ subarrays.

## 3. METHOD OF MULTI-DIRECTION SWATH IMAGING

Numerous practical applications of spaceborne SAR are required for the repeated acquisition and dynamic monitoring of some different ground areas at the same time. Fig. 2 shows the Hybrid Phased-MIMO SAR acquisition geometry with four subarrays. For this system, all subarrays will be activated to emit subpulses in succession by dividing the total transmit pulse into multiple subpulses with an interval $T_0$ that is the transmit interval between two subpulses, where the number of subpulses corresponds to the number of subarrays forming the subbeams towards different swaths $W_k$ [23], and the equation can then be written as

$$W_k = \frac{Tc}{2\sin\varphi_k} \tag{9}$$

where $T$ is the subpulse duration, $\varphi_k$ the incident angle, and $H$ the satellite altitude.

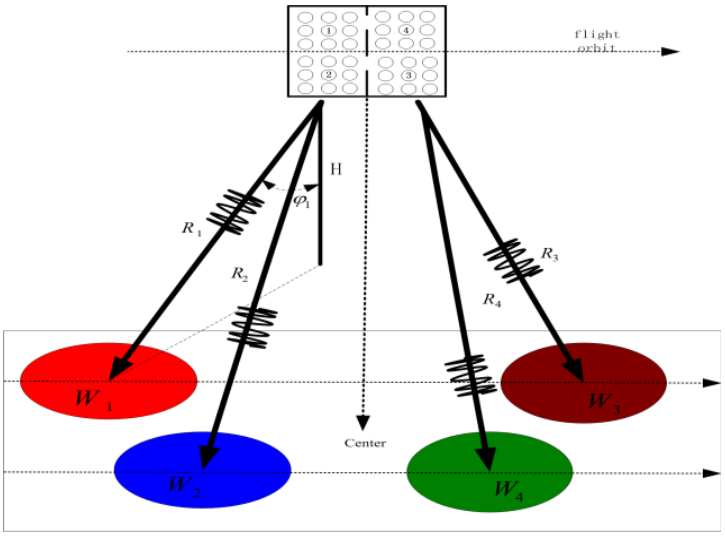


**Figure 2.** Multi-direction SAR acquisition geometry.

### 3.1. Signal Model

In Section 2, $\tilde{s}_k(t)$ is the linear frequency modulation (LFM) signal in (3) and can be expressed as

$$\tilde{s}_k(t) = rect\left[\frac{t-(k-1)T_0}{T}\right]\exp\left\{j2\pi f_0\left[t-(k-1)T_0\right]+j\pi k_r\left[t-(k-1)T_0\right]^2\right\} \tag{10}$$

where $k_r$ is the chirp rate. We utilize generic point-like target model to analyze the received raw data. Suppose that every swath corresponds to a point target with different slant ranges $R_1$, $R_2$, ..., $R_k$ satisfying

$$\begin{aligned}\frac{2R_1}{c} &= \frac{2R_2}{c}+T_0\\ \frac{2R_2}{c} &= \frac{2R_3}{c}+T_0\\ &\vdots\\ \frac{2R_{k-1}}{c} &= \frac{2R_k}{c}+T_0\end{aligned} \tag{11}$$

For the $k$th point target, its corresponding echo is given by

$$\mathbf{s}_{out\_k}\left(t-2R_k/c\right)=\sqrt{E_k}\tilde{s}_{out\_k}\left(t-2R_k/c\right)\mathbf{w}_k^*,\quad k=1,\ldots,M \tag{12}$$

with

$$\tilde{s}_{out\_k}\left(t-2R_k/c\right)=\rho_t rect\left[\frac{t-2R_{k-1}/c}{T}\right]\exp\left\{j2\pi f_0\left[t-2R_{k-1}/c\right]+j\pi k_r\left[t-2R_{k-1}/c\right]^2\right\} \tag{13}$$

where $\rho_t$ is the target reflection amplitude. Each subarray $j$ responds to the composite reflected signal from different point targets, and these received signals can be written as

$$\mathbf{r}_j\left(t-2R_k/c\right)=y\left(t-2R_k/c\right)\mathbf{a}_j\left(\theta_k\right)=\sum_{k=1}^{M}\sqrt{E_k}\tilde{s}_{out\_k}\left(t-2R_k/c\right)\mathbf{w}_k^H\mathbf{a}_k\left(\theta_k\right)\mathbf{a}_j\left(\theta_k\right) \tag{14}$$

where $y(t-2R_k/c)$ is the echo signal of $y(t)$ in (7).

Suppose that the reflected signal from direction $\theta_k$ is received by the $j$th subarray, and it can be expressed as

$$\tilde{\mathbf{r}}_j\left(t-2R_k/c\right)=\sqrt{E_k}\tilde{s}_{out\_k}\left(t-2R_k/c\right)\mathbf{w}_k^H\mathbf{a}_k\left(\theta_k\right)\mathbf{a}_j\left(\theta_k\right) \tag{15}$$

Stacking all the received signals by $M$ subarrays into a signal vector, we have

$$\begin{aligned}\mathbf{r}\left(\theta_k\right)&=\begin{bmatrix}\tilde{\mathbf{r}}_1\left(\theta_k\right)\\ \vdots\\ \tilde{\mathbf{r}}_M\left(\theta_k\right)\end{bmatrix}\\&=\sqrt{E_k}\tilde{s}_{out\_k}\left(t-2R_k/c\right)\mathbf{A}^T\left(\theta_k\right)\otimes\mathbf{b}\left(\theta_k\right)\\&=\sqrt{E_k}\tilde{s}_{out\_k}\left(t-2R_k/c\right)\mathbf{P}\left(\theta_k\right)\end{aligned} \tag{16}$$

where $\otimes$ stands for the kronecker product, $\mathbf{b}(\theta_k)=\mathbf{w}_k^H\mathbf{a}_k(\theta_k)$, and $\mathbf{P}(\theta_k)$ is the $N\times M$ virtual steering matrix of the Hybrid Phased-MIMO SAR as

$$\mathbf{P}\left(\theta_k\right)=\begin{bmatrix}\mathbf{b}\left(\theta_k\right) & \cdots & \mathbf{b}\left(\theta_k\right)\\ \mathbf{b}\left(\theta_k\right)e^{-j2\pi f_0 d\cos\theta_k/c} & \cdots & \mathbf{b}\left(\theta_k\right)e^{-j2\pi f_0\cos\theta_k/c}\\ \vdots & \cdots & \vdots\\ \mathbf{b}\left(\theta_k\right)e^{-j2\pi f_0(N-1)d\cos\theta_k/c} & \cdots & \mathbf{b}\left(\theta_k\right)e^{-j2\pi f_0(N-1)d\cos\theta_k/c}\end{bmatrix}^T \tag{17}$$

In the final expression, we can achieve multi-direction swath imaging with an appropriate $\mathbf{P}(\theta_k)$, and the echo signal power of the direction $\theta_k$ is the strongest. The great echoes from multiple swaths will produce a large number of overlapped echoes from different subpulses in the range time domain and serious range ambiguities, resulting in terrible image. We will provide our advanced beamforming approach to cope with these problems in the next section.

### 3.2. Advanced Algorithm of Adaptive DBF

Figure 3 shows this phenomenon with a simple two-subpulse system corresponding to the images $W_1$ and $W_2$. One can observe the overlapping area $U_1$ in the range time. This is just an abridged general view without serious range ambiguity. It is worth noting that echoes from various subpulses have been partially overlapped in the range time domain, but the spatial information contained in them is

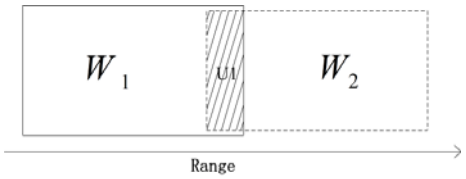


**Figure 3.** Range position of raw data blocks

significantly different at any instant within the receiving window since they are always from different positions and looking angles. Therefore, it is possible to separate them and suppress the range ambiguity via the approach of adaptive DBF in the spatial domain.

In [24–27], the technique of linear constraints minimum variance beamforming was proposed to assure proper reception of the desired signal. In this paper, we give an advanced adaptive DBF to separate overlapped echoes and suppress the range ambiguity.

Assuming that the target of interest is observed in the background of $B$ interfering targets with reflection coefficients $\{\rho_m\}_{m=1}^{B}$, locations $\{\theta_m\}_{m=1}^{B}$ and white Gaussian noise with the power $\sigma_n^2$. The $m$th echo signal can be written as

$$\begin{aligned}\mathbf{Q}_{out\_m}(t-2R_m/c) &= \sqrt{E_m}\rho_m\mathbf{w}_m^* rect\left[\frac{t-2R_{m-1}/c}{T}\right]\exp\left\{j2\pi f_0\left[t-2R_{m-1}/c\right]+j\pi k_r\left[t-2R_{m-1}/c\right]^2\right\}\\ &= \sqrt{E_m}\tilde{Q}_{out\_m}(t-2R_m/c)\,\mathbf{w}_m^*\end{aligned} \tag{18}$$

where

$$\tilde{Q}_{out\_m}(t-2R_m/c) = \rho_m rect\left[\frac{t-2R_{m-1}/c}{T}\right]\exp\left\{j2\pi f_0\left[t-2R_{m-1}/c\right]+j\pi k_r\left[t-2R_{m-1}/c\right]^2\right\} \tag{19}$$

and the received complex vector of array observations can be written as

$$\begin{aligned}\mathbf{X}(t) &= \mathbf{r}(\theta_k)+\sum_{m=1}^{B}\mathbf{z}(\theta_m)+\mathbf{n}(t)\\ &= \sqrt{E_k}\tilde{s}_{out\_k}(t-2R_k/c)\,\mathbf{P}(\theta_k)+\sum_{m=1}^{B}\sqrt{E_m}\tilde{Q}_{out\_m}(t-2R_m/c)\,\mathbf{P}(\theta_m)+\mathbf{n}(t)\end{aligned} \tag{20}$$

where $\mathbf{z}(\theta_m)$ is interference signal vector with respect to range ambiguity and adjacent subpulse echoes, $\mathbf{n}(t)$ the system noise vector of HMPAR, and $E_k = E_m = 1$ can be derived from (4).

A linearly constrained beamformer can be formulated as that of finding the weight vector $\mathbf{W}$ which minimizes the output power

$$\min_{\mathbf{W}}\mathbf{W}^H\mathbf{R}_{XX}\mathbf{W} \quad s.t. \quad \mathbf{C}^H\mathbf{W}=\mathbf{f} \tag{21}$$

where $\mathbf{R}_{XX}$ is the interference-plus-noise covariance matrix, $\mathbf{C}$ the constraint matrix, and the vector $\mathbf{f}$ specifies the corresponding constraint value for each vector.

It is well known that the optimal solution of the minimization problem defined above is

$$\mathbf{W}_{opt} = \mathbf{R}_{XX}^{-1}\mathbf{C}\left(\mathbf{C}^H\mathbf{R}_{XX}^{-1}\mathbf{C}\right)^{-1}\mathbf{f} \tag{22}$$

And then we will design $\mathbf{C}$, $\mathbf{f}$ and $\mathbf{R}_{XX}^{-1}$ appropriately, where $\mathbf{C}$ includes three parts, and their analytical expressions have the form

$$\mathbf{C} = \left[\begin{array}{ccc}\bar{\mathbf{W}}_0 & \bar{\mathbf{C}}_0 & \mathbf{A}(\theta_m)\end{array}\right] \tag{23}$$

and

$$\mathbf{f} = \left[\begin{array}{cccc}1 & 0 & \cdots & 0\end{array}\right]^T \tag{24}$$

$$\bar{\mathbf{W}}_0 = \frac{\mathbf{W}_0}{\mathbf{W}_0^H\mathbf{W}_0} \tag{25}$$

where $\mathbf{W}_0$ is the weighting coefficients of the desired quiescent response, $\bar{\mathbf{C}}_0$ to prevent the desired signal from being cancelled by adaptive weights and shown in [28], and $\mathbf{A}(\theta_m)$ the steering vector matrix of interference signal. We want to achieve desired quiescent response with an overall low sidelobe and $B$ nulls at the jammer direction.

Suppose that there are $N$ elements for reception and that the covariance inverse matrix is expressed in the terms of feature space theory as follows

$$\mathbf{R}_{XX}^{-1} = \sum_{i=1}^{B}\lambda_i^{-1}e_ie_i^H + \sum_{i=B+1}^{N}\sigma_n^{-2}e_ie_i^H = \sigma_n^{-2}\left[\mathbf{I}-\sum_{i=1}^{N}\frac{\lambda_i-\sigma_n^2}{\lambda_i}e_ie_i^H\right] \tag{26}$$

where $e_i$ is the eigenvector of $\mathbf{R}_{XX}$, and $\lambda_i$ corresponds to its eigenvalue. In order to achieve the desired adaptive low sidelobe and reduce the small eigenvalue interference for its eigenvector, we apply the technique of diagonal loading in [29], which adds an appropriate value $Q$ to every eigenvalue. So the expression (22) can be rewritten as

$$\mathbf{W}_{opt} = \left[\mathbf{I} - \sum_{i=1}^{N} \frac{\lambda_i + Q - \sigma_n^2}{\lambda_i + Q} e_i e_i^H\right] \bar{\mathbf{C}} \left(\overline{\bar{\mathbf{C}}^H \left[\mathbf{I} - \sum_{i=1}^{N} \frac{\lambda_i + Q - \sigma_n^2}{\lambda_i + Q} e_i e_i^H\right] \bar{\mathbf{C}}}\right)^{-1} \mathbf{f} \tag{27}$$

The output of the Hybrid Phased-MIMO SAR system after the adaptive DBF is given by

$$\begin{aligned}
\mathbf{Y}(t) &= \mathbf{W}_{opt}^H \mathbf{X}(t) \\
&= \tilde{s}_{out_k}(t - 2R_k/c)\, \mathbf{W}_{opt}^H \mathbf{P}(\theta_k) + \sum_{m=1}^{B} \tilde{Q}_{out_m}(t - 2R_m/c)\, \mathbf{W}_{opt}^H \mathbf{P}(\theta_m) + \mathbf{N}(t) \\
&= \tilde{s}_{out_k}(t - 2R_k/c)\, \mathbf{U}(\theta_k) + \sum_{m=1}^{B} \tilde{Q}_{out_m}(t - 2R_m/c) \mathbf{U}(\theta_m) + \mathbf{N}(t)
\end{aligned} \tag{28}$$

where $\mathbf{U}(\theta_k) = \mathbf{W}_{opt}^H \mathbf{P}(\theta_k)$ is the channel steering vector of the desired signal from direction $\theta_k$, $\mathbf{U}(\theta_m) = \mathbf{W}_{opt}^H \mathbf{P}(\theta_m)$ the channel steering vector of the interference signal from direction $\theta_m$, and $\mathbf{N}(t)$ the noise after optimal weighting.

### 3.3. System Design of the Hybrid Phased-MIMO SAR

In this section, we will present a system design example of spaceborne Hybrid Phased-MIMO SAR in elevation dimension, as shown by the system structure of our digital beamformer in Fig. 4. The system transmits $M$ subpulses forming different direction subbeams to cover $M$ swaths and receives echoes from every swath by $M$ subarrays at the same time. We will separate the overlapped image shown in Fig. 3 caused by overlapped echoes from the two adjacent subpulses in the range time domain through the separation for the $(M-1)$th subpulse and the $M$th subpulse. Received signals after A/D converter will be weighted by the corresponding optimal weight vector $\mathbf{W}_{optM-1}^H$ and $\mathbf{W}_{optM}^H$ derived in (27) and then combined to extract the echoes from the $M$th subpulse. Finally, the echoes of these subpulses pass through the corresponding matched filter $H(f)$ to achieve the non-overlapped images $M$ and $(M-1)$

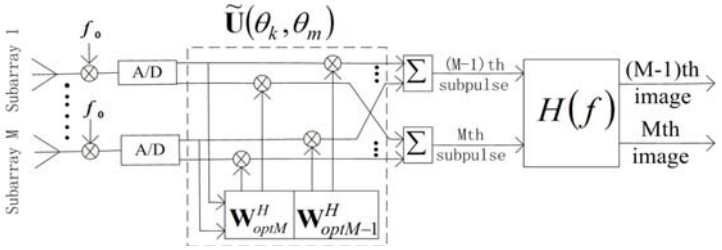


**Figure 4.** Block diagram of system design.

**Table 2.** System parameters used in the simulation.

| PARAMETER | VALUE | PARAMETER | VALUE |
|---|---|---|---|
| Orbit Height | 576 km | Number of Subpulses | 2 |
| Sub-swath | 2 | Subpulse Duration | 50 μs |
| Bandwidth | 100 MHz | Number of Subarrays in Elevation | 2 |
| Carrier Frequency | 9.65 GHz | Number of Subapertures in Elevation | 100 |

with the pulse compression in the range before the adders in our digital beamformer, where $\tilde{\mathbf{U}}(\theta_k, \theta_m)$ is the system channel steering vector of the echo signals and given by

$$\tilde{\mathbf{U}}(\theta_k, \theta_m) = \begin{cases} \mathbf{U}(\theta_k), & k = m \\ \mathbf{U}(\theta_m), & k \neq m \end{cases} \tag{29}$$

We ignore the constant exponential term $\exp\{-\mathrm{j}(4\pi f_0 R_{k-1}/c)\}$ in (13) and $\exp\{-\mathrm{j}(4\pi f_0 R_{m-1}/c)\}$ in (19) due to the irrelevance to the subsequent processing.

Then, after $\mathbf{Y}(t)$ have been down converted one can obtain its corresponding spectrum as

$$\begin{aligned} \mathbf{Y}(f) \approx{}& \rho_t^3 rect\left[\frac{f}{k_r T}\right] \exp\left\{-j\pi\frac{f^2}{k_r}\right\} \exp\{-j4\pi f R_{k-1}/c\}\, \mathbf{U}(\theta_k) \\ &+ \sum_{m=1}^{B} \rho_t^2 \rho_m rect\left[\frac{f}{k_r T}\right] \exp\left\{-j\pi\frac{f^2}{k_r}\right\} \exp\{-j4\pi f R_{m-1}/c\}\, \mathbf{U}(\theta_m) + FFT\{\mathbf{N}(t)\} \end{aligned} \tag{30}$$

where $FFT$ stands for Fourier transform. The system matched filter $H(f)$ can be expressed as

$$H(f) = \mathrm{rect}\left[\frac{f}{k_r T}\right] \exp\{j\pi f^2/k_r\} \tag{31}$$

From the previously obtained result of $\mathbf{Y}(f)$ after matched filter processing and transforming back into the time domain, we can get

$$\mathbf{y}_{out}(t) = A_t \mathbf{U}(\theta_k) \sin c(\Delta f_t (t - 2R_{k-1}/c)) + \sum_{m=1}^{B} A_m \mathbf{U}(\theta_m) \sin c(\Delta f_t (t - 2R_{m-1}/c)) + \tilde{\mathbf{N}}(t) \tag{32}$$

where $A_t$ and $A_m$ are constant, and $\Delta f_t$ is the bandwidth of subpulse. From the final expression (32), we can achieve the desired image in the range time domain.

## 4. SIMULATION RESULTS

In this paper, we have given the theoretical derivation of the Hybrid Phased-MIMO SAR, and then we will present the simulation results of DBF in elevation and the system parameters that will be used in the following simulations in Table 2. Consider a spaceborne Hybrid Phased-MIMO SAR system equipped with two subarrays in elevation, the bandwidth of the LFM signal is 100 MHz which is divided into two subpulses with interval $T_0$, and the corresponding two swaths are located at directions $\theta_1$ and

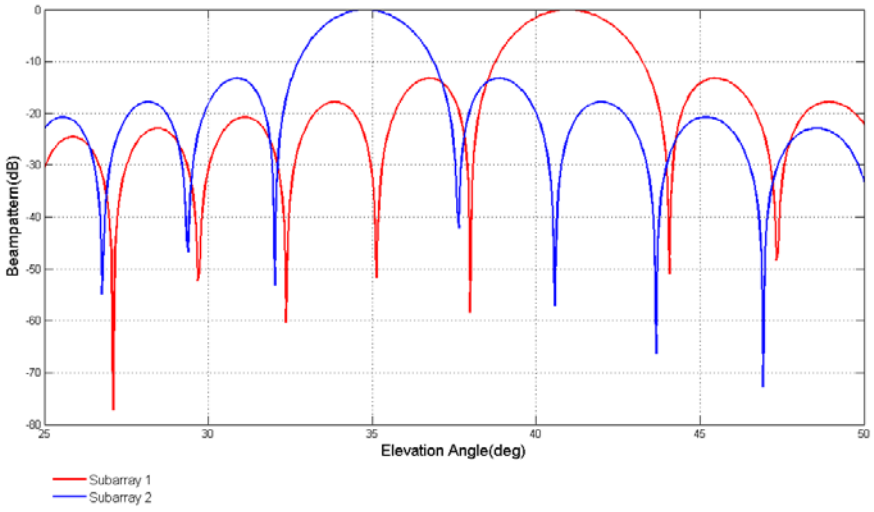


**Figure 5.** Bidirectional beampattern in elevation.

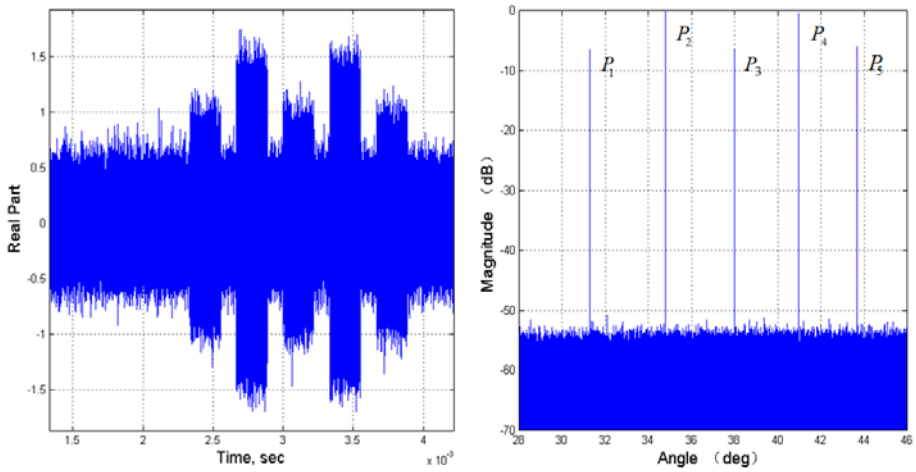


**Figure 6.** Raw data without beamforming for four point targets. (a) Real part. (b) Range compression result.

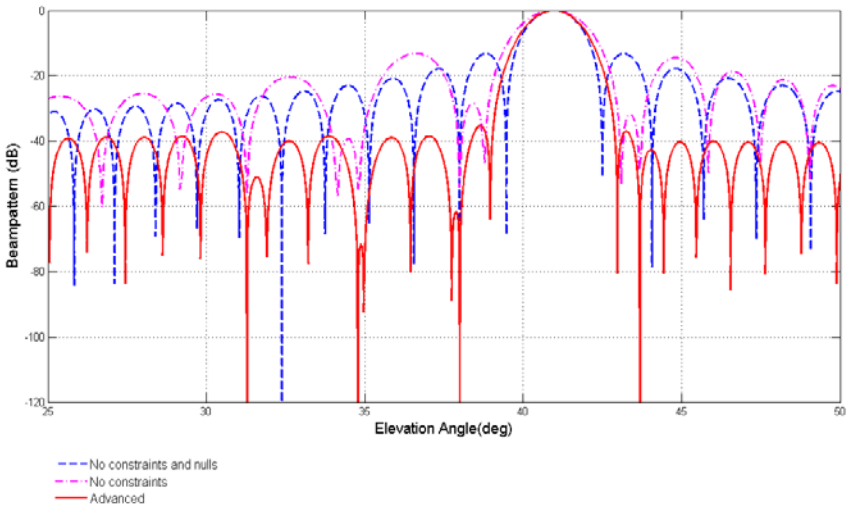


**Figure 7.** Beampattern for direction 40.96°.

$\theta_2$. Fig. 5 shows the bidirectional beampattern in elevation and the two beams towards 34.78° and 40.96°, respectively.

Figure 6 shows the compression results in range without adaptive DBF algorithm. $P_2$, $P_4$ are the desired signals corresponding to the two subpulses, but they will be overlapped at the receiving side. $P_1$, $P_3$, $P_5$ are the range ambiguity with high magnitude and located at 31.28°, 38° and 43.68°, respectively. Comparing with desired signals, we will suppress these interference signals with enough lower level and separate the two desired signals. In Fig. 7 and Fig. 8, by comparing the beampatterns at receiving, the blue line is conventional beamforming without constraints and nulls, and the pink one is conventional null-steering beamforming without constraints. It can be seen that the red line has a $-40$ dB uniform sidelobe level approximately and sets four nulls located at 31.28°, 34.78°, 38° and 43.68° in Fig. 7, and at 31.28°, 38°, 40.96° and 43.68° in Fig. 8. From the results, we can see that our adaptive DBF approach works well for the beampattern at the receiving.

Next, we compare the separation performance and suppression performance associated with three kinds of beamformers. The corresponding results are shown in Figs. 9–14. Independent white noise has been added to each subaperture signal, and the signal-to-noise ratio (SNR) is 20 dB. Further investigations were carried out to evaluate the sensitivity for the noise. Conventional null-steering beamforming is influenced greatly by the noise power. When the noise power is bigger, its suppression

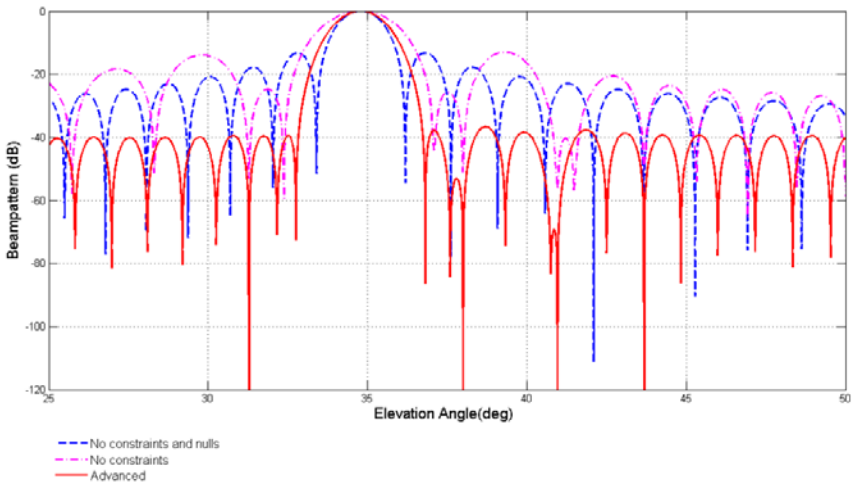


**Figure 8.** Beampattern for direction 34.78°.

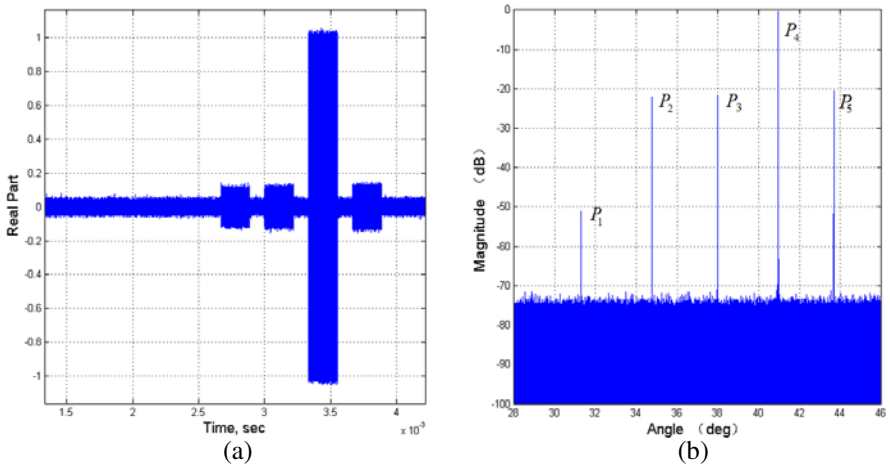


**Figure 9.** Conventional beamforming without nulls and constraints for the point target $P_4$. (a) Real part of the suppressed echoes. (b) Range compression result of the suppressed echoes.

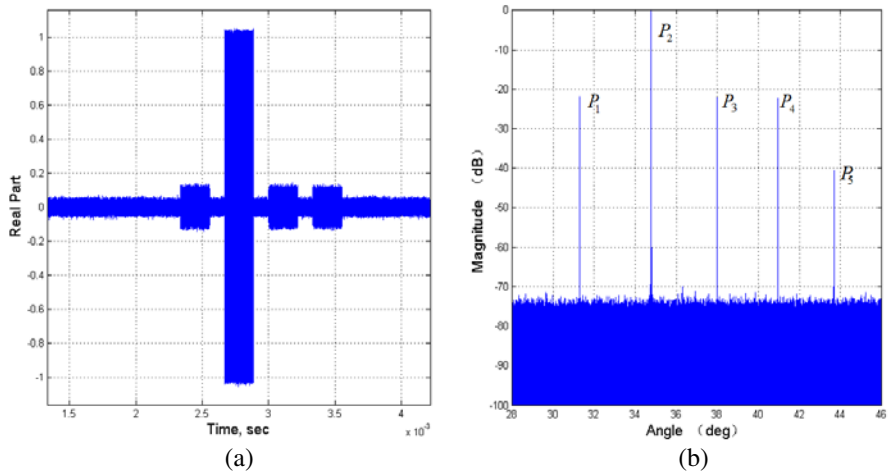


**Figure 10.** Conventional beamforming without nulls and constraints for the point target $P_2$. (a) Real part of the suppressed echoes. (b) Range compression result of the suppressed echoes.

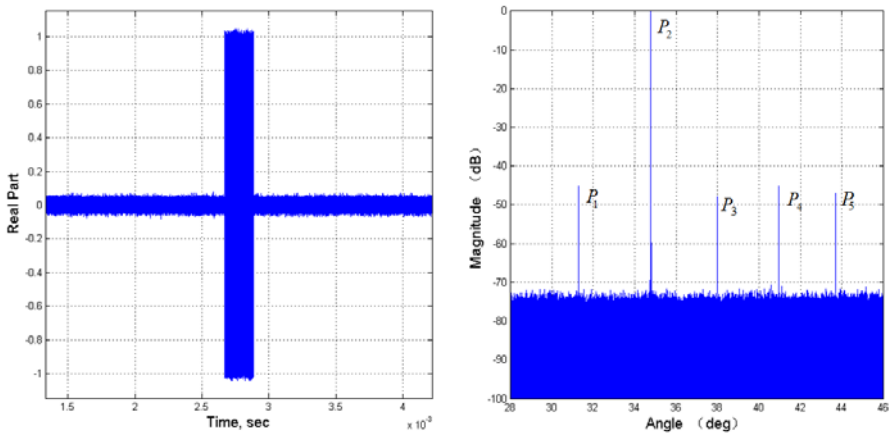


(a) (b)

**Figure 11.** Conventional null-steering beamforming without constraints for the point target $P_2$. (a) Real part of the suppressed echoes. (b) Range compression result of the suppressed echoes.

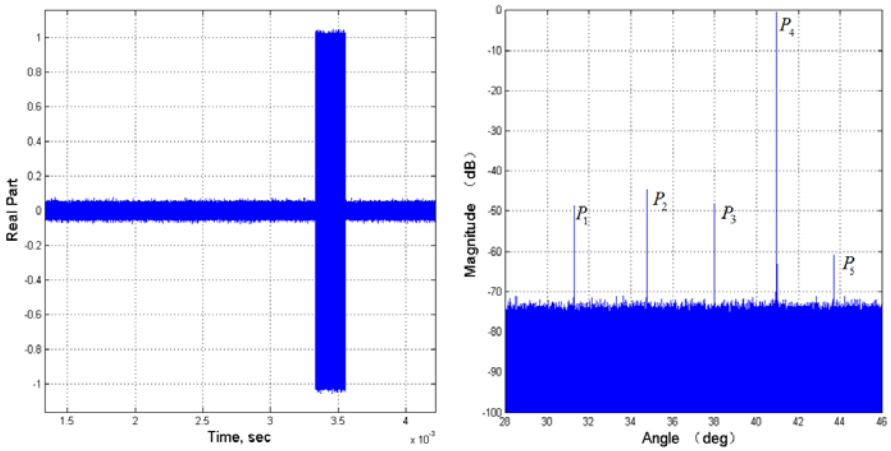


(a) (b)

**Figure 12.** Conventional null-steering beamforming without constraints for the point target $P_4$. (a) Real part of the suppressed echoes. (b) Range compression result of the suppressed echoes.

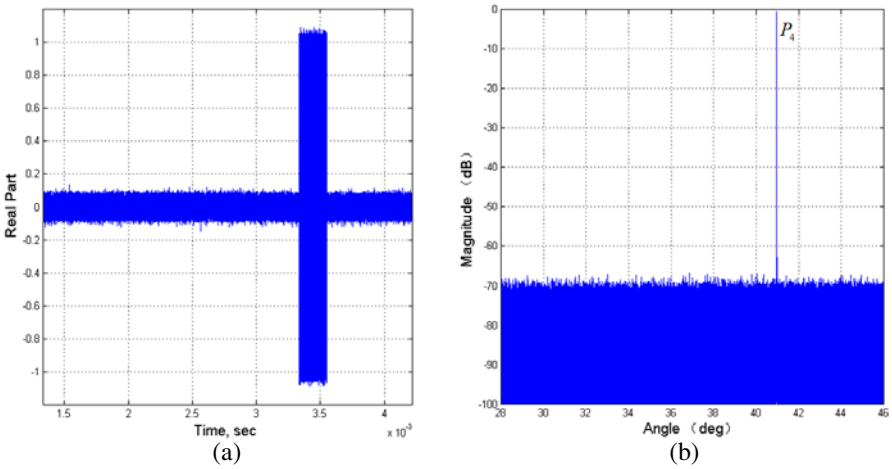


(a) (b)

**Figure 13.** Advanced beamforming for the point target $P_4$. (a) Real part of the suppressed echoes. (b) Range compression result of the suppressed echoes.

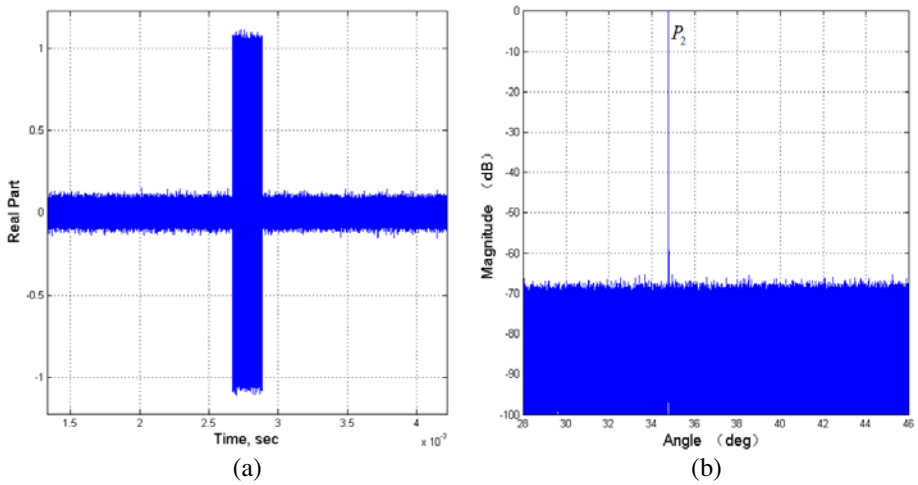


**Figure 14.** Advanced beamforming for the point target $P_2$. (a) Real part of the suppressed echoes. (b) Range compression result of the suppressed echoes.

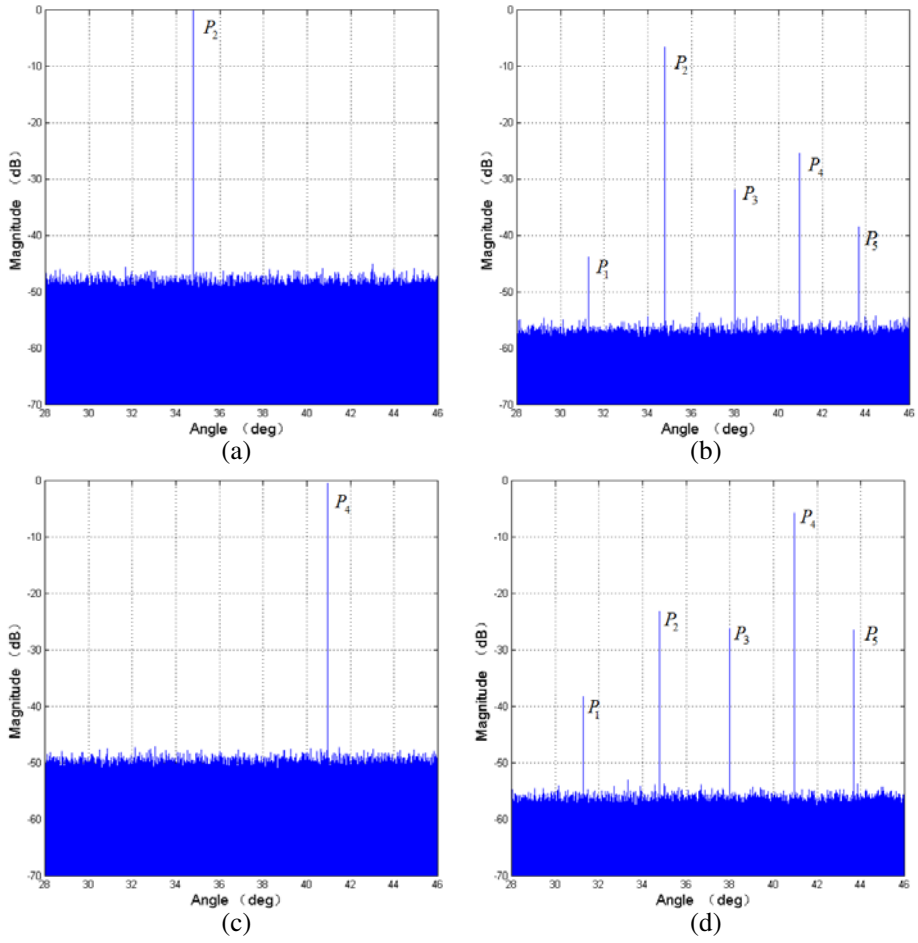


**Figure 15.** Performance of advanced beamforming and conventional null-steering beamforming at SNR = 0 dB. (a) Range compression result of advanced beamforming for the point target $P_2$. (b) Range compression result of conventional null-steering beamforming for the point target $P_2$. (c) Range compression result of advanced beamforming for the point target $P_4$. (d) Range compression result of conventional null-steering beamforming for the point target $P_4$.

performance declines obviously, as shown in Fig. 15. From the above simulation results we can conclude that our advanced beamforming provides efficient and stable interference suppression. As a result, overlapped echoes can be separated easily.

## 5. CONCLUSION

This paper has presented the method of multi-direction swath imaging based on spaceborne Hybrid Phased-MIMO SAR which can be satisfied with the next generation of top-level spaceborne SAR to achieve various functions by controlling transmit beampatterns. Orthogonal signals are used with the subarrays beams pointed in different directions. For the overlapped image in range caused by adjacent subpulse, we present the advanced algorithm of adaptive DBF in elevation. An important feature of this method is that it allows the quiescent response of the beamformer to be specified as any desirable fixed-weight response. The additional constraints are included to assure proper reception of the desired signal and form nulls in the direction of interference at the same time. Compared with conventional beamformings, our approach shows efficient and stable interference suppression, and the simulation results show its validation. The corresponding Hybrid Phased-MIMO SAR two-dimensional DBF, analysis of specific parameters, and chirp modulation diversity waveform design will be further investigated in subsequent work.

## ACKNOWLEDGMENT

The authors would like to thank the editor and anonymous reviewers for their valuable time, comments, and suggestions to improve the quality and readability of this paper.

## REFERENCES

1. Gebert, N., G. Krieger, and A. Moreira, "Multichannel azimuth processing in scanSAR and TOPS mode operation," *IEEE Transactions on Geoscience and Remote Sensing*, Vol. 48, No. 7, 2994–3008, 2010.
2. Gao, C., R. Wang, Y. Deng, et al., "Large-scene sliding spotlight SAR using multiple channels in azimuth," *IEEE Geoscience and Remote Sensing Letters*, Vol. 10, No. 5, 1006–1010, 2013.
3. Guo, D., H. Xu, and J. Li, "Extended wavenumber domain algorithm for highly squinted sliding spotlight SAR data processing," *Progress In Electromagnetics Research*, Vol. 114, 17–32, 2011.
4. An, D. X., Z.-M. Zhou, X.-T. Huang, and T. Jin, "A novel imaging approach for high resolution squinted spotlight SAR based on the deramping-based technique and azimuth NLCS principle," *Progress In Electromagnetics Research*, Vol. 123, 485–508, 2012.
5. Park, S.-H., J.-I. Park, and K.-T. Kim, "Motion compensation for squint mode spotlight SAR imaging using efficient 2D interpolation," *Progress In Electromagnetics Research*, Vol. 128, 503–518, 2012.
6. Henke, D., C. Magnard, M. Frioud, et al., "Moving-target tracking in single-channel wide-beam SAR," *IEEE Transactions on Geoscience and Remote Sensing*, Vol. 50, No. 11, 4735–4747, 2012.
7. Wollstadt, S., P. Prats-Iraola, P. Lopez-Dekker, et al., "Bidirectional SAR imaging mode," *IEEE Transactions on Geoscience and Remote Sensing*, Vol. 51, No. 1, 601–614, 2013.
8. Huber, S., M. Younis, A. Patyuchenko, et al., "Digital beam forming techniques for spaceborne reflctor SAR systems," *Synthetic Aperture Radar (EUSAR)*, 1–4, 2010.
9. Huber, S., M. Younis, A. Patyuchenko, et al., "Digital beam forming concepts with application to spaceborne reflector SAR systems," *International Radar Symposium (IRS)*, 1–4, 2010.
10. Krieger, G., N. Gebert, M. Younis, et al., "Advanced concepts for ultra-wide-swath SAR imaging," *Synthetic Aperture Radar (EUSAR)*, 1–4, 2008.
11. Ender, J. H. G. and A. R. Brenner, "PAMIR — A wideband phased array SAR/MTI system," *IEE Proceedings Radar, Sonar and Navigation*, Vol. 150, No. 3, 165–172, 2003.

12. Ludwig, M., C. H. Buck, F. Coromina, and M. Suess, "Status and trends for space-borne phased array radar (INVITED)," *IEEE MTT-S International Microwave Symposium Digest*, 2005.
13. Krieger, G., N. Gebert, and A. Moreira, "Multidimensional radar waveforms," *Geoscience and Remote Sensing Symposium*, 4937–4941, Barcelona, 2007.
14. Krieger, G., N. Gebert, M. Younis, and A. Moreira, "Advanced synthetic aperture radar based on digital beamforming and waveform diversity," *Radar Conference*, 1–6, Rome, 2008.
15. Krieger, G., N. Gebert, and A. Moreira, "Multidimensional waveform encoding: A new digital beamforming technique for synthetic aperture radar remote sensing," *IEEE Transactions on Geoscience and Remote Sensing*, Vol. 46, No. 1, 31–46, 2008.
16. Browning, J. P., D. R. Fuhrmann, and M. Rangaswamy, "A hybrid MIMO phased-array concept for arbitrary spatial beampattern synthesis," *IEEE Digital Signal Processing and Signal Processing Education Workshop (DSP/SPE'09)*, 446–450, Marco Island, FL, 2009.
17. Hassanien, A. and S. A. Vorobyov, "Phased-MIMO radar: A tradeoff between phased-array and MIMO radars," *IEEE Transactions on Signal Processing*, Vol. 58, No. 6, 1–33, 2010.
18. Fuhrmann, D. R., J. P. Browning, and M. Rangaswamy, "Signaling strategies for the hybrid MIMO phased-array radar," *IEEE Journal of Selected Topics in Signal Processing*, Vol. 4, No. 1, 66–78, 2010.
19. Hua, G. and S. S. Abeysekera, "Receiver design for range and doppler sidelobe suppression using MIMO and phased-array radar," *IEEE Transactions on Signal Processing*, Vol. 61, No. 6, 1315–1326, 2013.
20. Wang, W.-Q. and H. Shao, "A flexible phased-MIMO array antenna with transmit beamforming," *International Journal of Antennas and Propagation*, 1–10, 2012.
21. Feng, F., S. Li, W. Yu, P. Huang, and W. Xu, "Echo separation in multidimensional waveform encoding SAR remote sensing using an advanced null-steering beamformer," *IEEE Transactions on Geoscience and Remote Sensing*, Vol. 50, No. 10, 4157–4171, 2012.
22. Krieger, G., M. Younis, S. Huber, et al., "Digital beamforming and MIMO SAR: Review and new concepts," *Synthetic Aperture Radar*, 11–14, 2012.
23. Kou, G., Z. Wang, and P. Yao, "Multiple beams spaceborne SAR imaging," *IEEE Transactions on Aerospace and Electronic Systems*, Vol. 48, No. 4, 3363–3375, 2012.
24. Tseng, C.-Y. and L. J. Griffiths, "A simple algorithm to achieve desired patterns for arbitrary arrays," *IEEE Transaction on Signal Processing*, Vol. 40, No. 11, 2737–2746, 1992.
25. Tseng, C.-Y. and L. J. Griffiths, "A unified approach to the design of linear constraints in minimum variance adaptive beamformers," *IEEE Transactions on Antennas and Propagation*, Vol. 40, No. 12, 1533–1542, 1992.
26. Shi, Z. and Z. Feng, "A new array pattern synthesis algorithm using the two-step least-squares method," *IEEE Signal Processing Letters*, Vol. 12, No. 3, 250–253, 2005.
27. Wang, F., R. Yang, and C. Frank, "A new algorithm for array pattern synthesis using the recursive least squares method," *IEEE Signal Processing Letters*, Vol. 10, No. 8, 235–238, 2003.
28. Tseng, C.-Y., "Minimum variance beamforming with phase-independent derivative constraints," *IEEE Transactions on Antennas and Propagation*, Vol. 40, No. 3, 285–294, 1992.
29. Carlson, B. D., "Covariance matrix estimation errors and diagonal loading in adaptive arrays," *IEEE Transactions on Aerospace and Electronic Systems*, Vol. 24, No. 4, 397–401, 1988.